Ambient RF Energy Harvesting From a Two-Way Talk Radio for Flexible Wearable Wireless Sensor Devices Utilizing Inkjet Printing Technologies

Jo Bito, *Student Member, IEEE*, Jimmy G. Hester, *Student Member, IEEE*, and Manos M. Tentzeris, *Fellow, IEEE*

***Abstract*—A complete design and additive fabrication process of flexible wearable radio-frequency (RF) energy harvesters for off-the-shelf 2 W two-way talk radios utilizing inkjet printing technology is discussed in this paper. As a result of numerous output dc power measurements of fabricated proof-of-concept prototypes, a maximum output power of 146.9 mW and 43.2 mW was achieved with an H-field and E-field harvester, respectively. Also, the effect of misalignment between receiver and hand-held radio on harvesting performance is discussed in detail. To verify their potential in real-world wearable autonomous RF modules, the operation of E- and H-field energy harvesters was verified by utilizing an LED and a microcontroller communication module under on-body and on-bottle conditions, and the effect of the energy harvesters on the performance of the harvested communication systems was inspected through received power measurements in an anechoic chamber.**

***Index Terms*—Autonomous sensors, energy harvesting, flexible, inkjet printing, on-body, wearable.**

I. Introduction

In RECENT years, the desire for a "smart" society, which utilizes technologies such as large scale sensor networks, Internet of Things (IoT) and smart skins is getting increasingly higher. One of the biggest issues to realize the autonomous operation of these sensors and devices is power supply. In order to solve this problem, ambient energy harvesting technology has attracted the interest of the research community in the last couple of decades. There are many different types of potential energy sources for ambient energy harvesting such as solar, heat and vibration. Among them, ambient microwave energy harvesting, because of its inherent applicability even through opaque walls, making it potentially more available than other ambient energy sources. There are many different types of available microwave signals, especially in urban environments, such as VHF/UHF television and WiFi signals [1], [2], although typically their energy density is lower than other sources [3]. As the most fundamental implementation issues associated with the low energy density and the characteristics of Schottky diodes, which are commonly used for RF-dc conversion circuit implementation, it is very difficult to achieve a high enough output voltage that can drive external circuitry. In addition, most integrated circuits (ICs) require more energy than that required for normal operation when they need to activate from "cold start," which means equivalently that their load resistance becomes very low (typically below 1 kΩ), further complicating the turn-on of the ICs using RF energy harvesters. In order to alleviate this problem, for example, a charged capacitor is utilized to guarantee the start up of ICs [4]. However, there are some "hotspots" where RF energy is fairly high, which can possibly provide enough energy to turn on external circuitry from cold start without using any supplemental energy sources [5]. As an example, the two-way talk radio, which is a commonly used device for short-distance communication, does not use any base station and directly sends the signal to the other mobile devices. Therefore, it generates a relatively high RF power compared to other mobile communication electronics, especially in near field. In general, there is a limited number of technologies that are utilizing the near-field coupling for the purpose of wireless power transfer and the near-field communication, for example the strongly coupled coil configurations and the near-field RFIDs [6]–[8]. In these applications, both Transmitter (Tx) and Receiver (Rx) are arbitrary designed and do not use an ambient energy source. At the same time, most of the ambient energy harvesting circuits do not use the near-field coupling. Nevertheless, as already reported, it is possible to generate substantially high dc power out of the RF signals generated from handheld devices, such as a two-way talk radio [9], [10]. In this paper, a novel near-field RF energy harvesting circuit on a flexible substrate, that can be fabricated with inkjet printing technology, for wearable sensor applications as well as a further characterization of the near-field energy harvester under practical misaligned conditions and an operation test using a microcontroller are discussed in detail as an extension of previously reported results.

Manuscript received June 30, 2015; revised September 24, 2015; accepted October 17, 2015. Date of publication November 18, 2015; date of current version December 02, 2015. The work of J. Bito, J. G. Hester, and M. M. Tentzeris was supported in part by the National Science Foundation and the Defense Threat Reduction Agency. This paper is an expanded version from the IEEE MTT-S International Microwave Symposium, Phoenix, AZ, USA, May 17–22, 2015.

The authors are with the School of Electrical and Computer Engineering, Georgia Institute of Technology, Atlanta, GA, 30332-250 USA (e-mail: jbito3@gatech.edu).

Color versions of one or more of the figures in this paper are available online at http://ieeexplore.ieee.org.

Digital Object Identifier 10.1109/TMTT.2015.2495289

II. Inkjet Printing for Zero-Power Flexible Wearable Sensors

Additive manufacturing such as inkjet printing and 3-D printing is becoming increasingly popular in industry because of its environmentally friendly and low cost fabrication process features. These emerging fabrication techniques can potentially decrease significantly the number of fabrication steps, including the etching processes, and drastically improve the

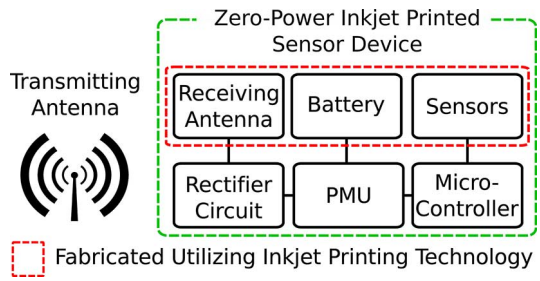

Fig. 1. Block diagram of a typical inkjet-printed zero-power wearable sensor device.

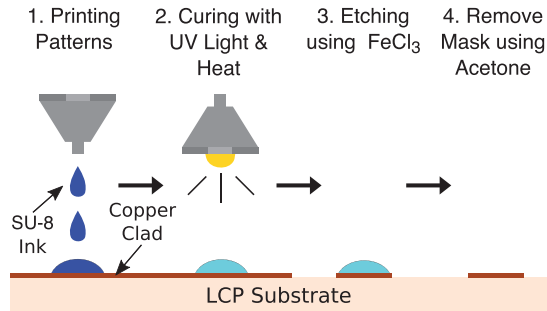

Fig. 2. Fabrication process of flexible circuit traces utilizing inkjet printing masking.

fabrication efficiency. Wearable sensor devices are expected to be used extensively in the places where single-time/disposable use is hygienically important, for example in hospitals. From this type of applications, it is desirable to create as many circuit components in the device as possible by utilizing additive manufacturing to reduce the cost of device. Due to recent substantial improvements in fabrication processes and performance, inkjet printing technology has become increasingly attractive for RF and sensor applications. As is depicted in Fig. 1, passive components, such as capacitors and inductors, circuit traces including antennas, battery, and sensors, can be created by utilizing printing technologies [11]–[16].

Inkjet printing technologies with silver nanoparticle-based inks have proven to be a very efficient solution for low-loss RF circuit patterning associated with a high 2-D resolution in the range of 50 to 100 μm [17]–[19]. However, it is quite challenging to fabricate durable flexible circuits with printed traces combined with lumped circuit components because of the limited flexibility of the conductive epoxy and the solder, that are commonly utilized as the electrical interconnect between inkjet-printed conductive patterns and circuit components. One of the options to overcome this problem is to create copper traces utilizing inkjet printing-based electroless electroplating, which enables to use conventional soldering to create electrical interconnections on flexible substrates [20]. However, because of the inevitable characteristic as a wearable device, it requires extra durability. In order to guarantee the interconnection under the wearing/flexing conditions, the masking through the use of an inkjet-printed polymer was adopted for the initial prototyping to prove the concept of near-field energy harvesting, and the research was extended to the fabrication of circuit utilizing inkjet-printed conductive traces. The Dimatix-2831 printing platform from Fujifilm was used to print both the masking layer and the conductive traces.

A. Inkjet Printing Masking

There are four steps in the fabrication of flexible circuit traces utilizing inkjet printing masking as are depicted in Fig. 2. The polymer ink is made of 35 w% SU-8 polymer from MicroChem, and was used as a mask on a copper-cladded liquid crystalline polymer (LCP) substrate from Rogers Corporation. The thickness and the dielectric constant of the substrate are 100 μm and 2.9, respectively. Once the SU-8 ink was printed on the copper cladding layer, the substrate was soft baked at 120 °C for 10 min before the masking was exposed to 365 nm ultraviolet (UV) light for cross linking. After the UV light exposure, the substrate was heated at 120 °C for additional 5 min, yielding

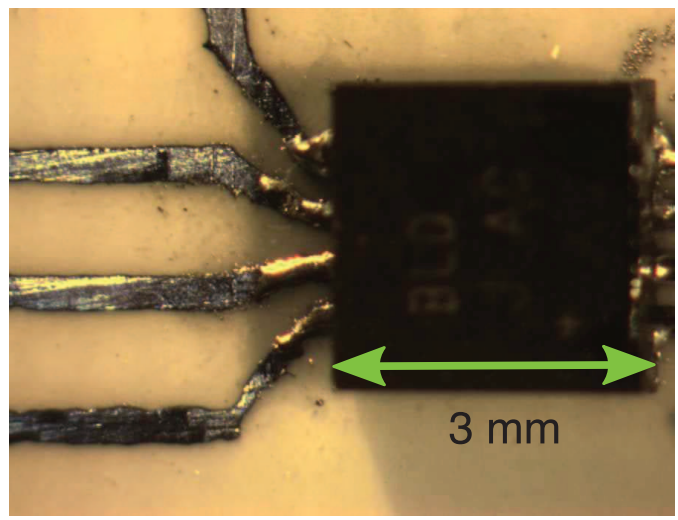

Fig. 3. Circuit traces for a TDFN8 IC package fabricated with inkjet printing masking.

a 4 to 6 μm SU-8 layer thickness [18]. Two layers of SU-8 were printed and then the uncovered copper metallization was etched with ferric chloride ($FeCl_3$) solution. The etching time varied from 30 to 90 min depending on the temperature, size of substrate, thickness of metal layer and freshness of the $FeCl_3$ solution. After the etching, SU-8 mask is removed by using acetone. Fig. 3 shows the printed conductive traces for a 3 mm $\times$ 3 mm TDFN8 package that have been fabricated with the above additive fabrication approach. The resolution of the conductive patterning is effectively equal to the resolution of inkjet printing, making it possible to fabricate circuit traces width and spacing of less than 400 μm for the prototype in Fig. 3, although narrower spacings below 90 μm can be easily realized, which is sufficiently good for many commonly used packaged ICs.

B. Inkjet Printed Conductive Traces

As an alternative additive manufacturing approach, the conductive traces for the wearable flexible harvesters introduced in this paper were printed by utilizing a silver nanoparticle-based ink, EMD5730 from SunChemical, which contains 40% silver nanoparticles diffused in an ethanediol-based solvent. This ink has a viscosity of 10 to 13 cPs at 25 °C and a surface tension of 27 to 31 dynes/cm [21]. Five layers of silver nanoparticle ink were printed on a 125 μm Kapton HN substrate from DuPont, which has the dielectric constant of 3.5. After the printing, the circuit was cured on a hotplate at 120 °C for 10 min after a

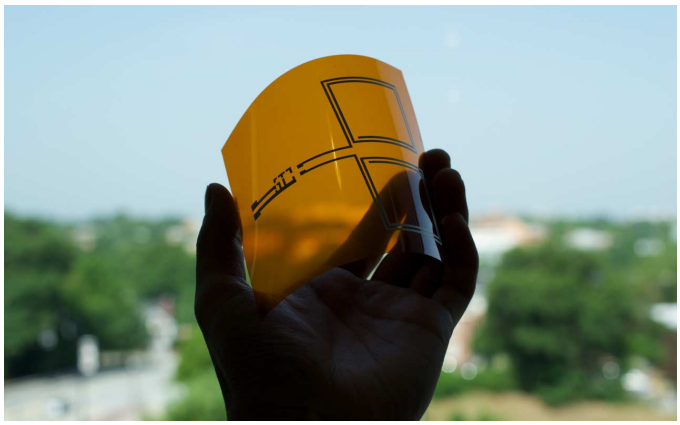

Fig. 4. Printed harvester circuit traces under bent/flex conditions.

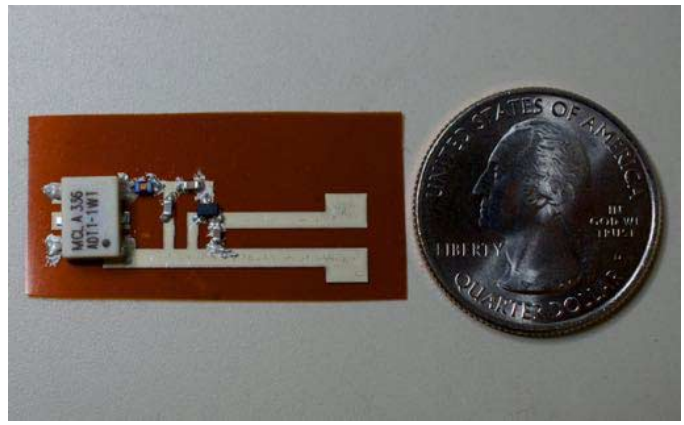

(a)

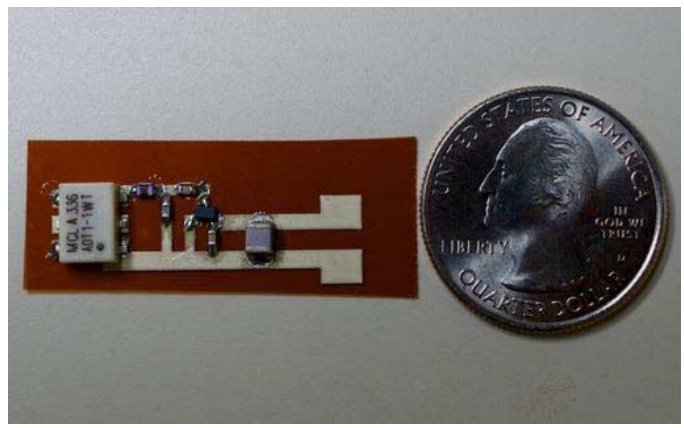

(b)

Fig. 5. (a) Interconnection using conductive epoxy. (b) Interconnection using low temperature soldering paste.

gradual temperature ramp from 30 °C with the rate of 360 °C per hour to dry the solvent in order to realize uniform printed conductive traces. After the initial curing, the circuit was heated at 150 °C for one hour, yielding 12-μm-thick layers at the center of a line with a sheet resistance of 0.011 Ω/sq. The curing temperature utilized is the lowest suggested curing temperature in the data sheet of the silver nanoparticle ink. This temperature was chosen in order to prevent the printed conductive traces from the cracks caused by the thermal expansion of the Kapton substrate. The conductivity of the printed traces is sufficiently high even with this relatively low-temperature curing [22]. The printed conductive traces themselves are as flexible as the Kapton substrate as depicted in Fig. 4. The inkjet-printed conductive traces are compatible with both conductive epoxy and low temperature soldering paste, which are typically used materials to make electrical connections to circuit traces and lumped components. The prototypes of the RF-dc conversion circuit using inkjet-printed conductive traces and lumped components which are soldered using the conductive epoxy and the low temperature soldering paste are shown in Fig. 5(a) and (b), respectively. The biggest issue of printed conductive traces for wearable applications in terms of mechanical properties is the stiffness difference between the conductive traces and the interconnection materials. This causes locally high mechanical stress on the edge of interconnections which eventually cracks the conductive traces when the circuit is bent. To alleviate this problem for wearable harvester applications, the RF-dc conversion circuit part in the fabricated prototype was laminated by utilizing a thin epoxy glue layer, which relieves the unequal stress distribution under bent/flexed conditions.

III. RF Power Measurements

In order to design a flexible wearable energy harvester circuit which can effectively scavenge energy from a hand-held radio, it is necessary to know the EM field distribution around the holding hand and to estimate how much is the input power to the harvesting circuit.

A. Near-Field Power Distribution Simulation and Measurement

In this paper, a Motorola RDU2020 two-channel two-way talk radio (2 W/1 W) was used as the power source and the radio was held with the right hand. The operation frequencies of this radio are 464.5500 MHz (Channel 1) and 467.9250 MHz (Channel 2), and the radio is utilizing Continuous Tone-Coded Squelch System (CTCSS) which is an analog squelch scheme in the factory setting. It is possible to switch the transmitting power of RDU2020 to 2 W and 1 W. In this research, 2 W mode and Channel 1 were used. The antenna of RDU2020 radio is not detachable, and the actual transmitted power from the radio cannot be directly measured. Therefore, another two-way talk radio, Motorola RDU4100, which can detach the antenna, was programmed to operate at 2 W mode and the output power was directly measured by utilizing a power sensor (NRP-Z211 from Rohde & Schwarz) and a 30 dB attenuator. Eventually, the actual measured transmitted power was 2.2 W. Therefore, in this paper, the transmitted power from RDU2020 radio is assumed to be 2.2 W. Since most people turn on the Walkie-Talkie with their hands, it is assumed that a sufficiently high amount of the output power in the near-field of the radio can be harvested by placing a harvester around the hand. In order to estimate the E- and H-field distribution around the hand holding the radio, various simulations were run on CST. In these simulations, a monopole antenna which has the same operation frequency as RDU2020 was placed near the thumb of the right-hand model which features the human flesh electrical properties. The simulation results of E- and H-field distribution on the back and on the palm sides are shown in Fig. 6. As it can be easily noticed, the E-field intensity is generally much higher than the

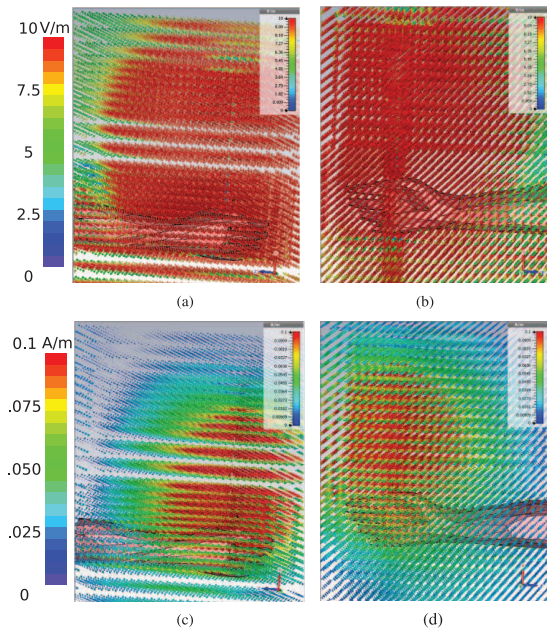

Fig. 6. E-field distribution of (a) Back side. (b) Palm side., and H-field distribution of (c) Back side. (d) Palm side.

H- field intensity, but there are some places where the H-field is locally high. In order to optimize the placement orientation of the wearable energy harvesting circuit, the intensity of electric and magnetic fields around the wrist were measured with an ETS-Lundgren E-field and H-field probe which was connected to a real-time spectrum analyzer, RSA3408A, from Tektronix. The measurement setup and the measured E- and H-field values at 2 to 17 cm away from the radio at various angular positions are shown in Fig. 7(a) and (b), respectively. It can also be concluded from these measurements that the electrical field is stronger than the magnetic field around the wrist. However, due to the typical near-field E-field distribution around a monopole antenna, the optimum E-field receiver needs to be placed parallel to the two-way radio antenna, which is difficult because of typical motions and changes in the relative positions of the radio in common holding arrangements of the radio near the wrist. On the other hand, the power level of the magnetic field at 0° position is relatively higher than any other angle; it is easier to increase the receiving area of the H-field by mounting the harvesting structure on the back of the hand, which is vertically facing the expected H-field, instead of placing the receiver on the wrist. Based on this assumption, receiver circuits for both electrical field and magnetic field were designed for proof-of-concept purposes.

B. E-Field and H-Field Receiver Design

By taking into account the typical size of a hand and a wrist, a width of 5 cm and length of 15 cm were adopted as the size constraints of the E-field receiver, and a width of 5 cm and a length of 8 cm were adopted for the H-field receiver . Based on the near-field power simulations and measurements, and the above wrist-dependent restrictions, receiver circuits for both E- and H-field were designed. A dipole antenna for E-field and an open-type helical coil with four loops for H-field were adopted at the

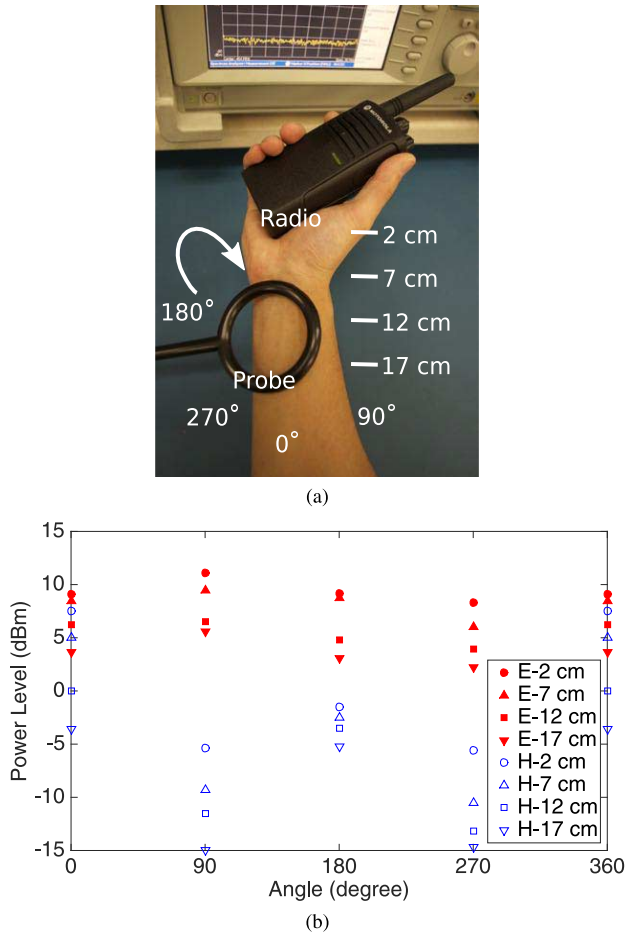

Fig. 7. (a) Near-field probe measurement configuration. (b) Measured E- and H-field power levels at different relative angles and distances.

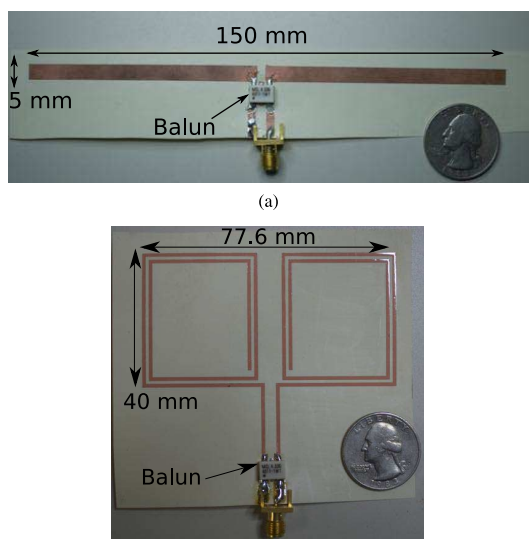

Fig. 8. Additively manufactured receiver prototypes for (a) E-field, (b) H-field.

wearable harvesting receiver. Both were soldered with the balun (ADT1-1WT) from Coilcraft Ink. The dimensions of the E- and the H-field receiver prototypes are shown in Fig. 8(a) and (b), respectively.

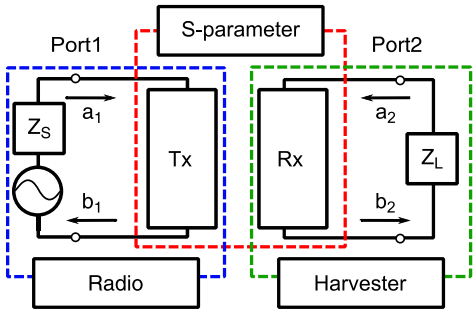

Fig. 9. System configuration with equivalent S-parameters matrix.

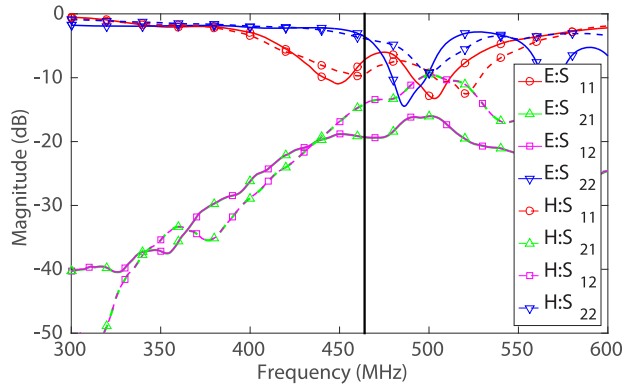

Fig. 10. Measured S-parameters for E- and H-field receivers.

C. Input Power Estimation and RF-DC Conversion Circuit Design

Since the transmitter and the receiver circuits are placed in the near field, it is very difficult to estimate how much power is actually transferred to the receiver through simulations. The requirement that the proposed receiver had to be wearable, as well as the detrimental proximity effect of the human body, further complicated this estimation. Therefore, in this paper, the power transferred to the receiver port was computed from two-port S-parameter measurements with a vector network analyzer (ZVA8 from Rohde & Schwarz). The energy harvesting system can be generally modeled as shown in Fig. 9. In this figure, Z_S is the source impedance and Z_L is the load impedance. If input and output power at port1 and port2 are defined as a_1, b_1, a_2, and b_2, respectively, the topology of the transmitter antenna and of the harvesting receiver can be expressed as a S-parameter matrix. Once the power transferred to the load and the power from the source, defined as P_L and P_S, respectively, the power transfer efficiency from the source to the load can be determined as shown in

$$\mu = \frac{P_L}{P_S} = \frac{b_2 b_2^* - a_2 a_2^*}{a_1 a_1^* + b_1 b_1^*} = \frac{(1-|\Gamma_L|^2)|S_{21}|^2}{|1-\Gamma_L S_{22}|^2}. \quad (1)$$

If the reflection coefficient from the source to port1 (Γ_{IN}) in (1) is substituted with

$$\Gamma_{IN} = S_{11} + \frac{\Gamma_L S_{21} S_{12}}{1-\Gamma_L S_{22}} \qquad Z_L = Z_0 \frac{1+\Gamma_L}{1-\Gamma_L} \quad (2)$$

the efficiency can be expressed only as a function of the reflection coefficient from port2 to the load (Γ_L). Therefore, once the two-port S-parameter matrix for the Tx-Rx propagation channel is calculated experimentally, the maximum power transfer efficiency can be analytically computed by sweeping the value of $\Gamma_L = Ae^{j\theta}$ in the range of $|A| = 1$ and $\theta = 0$ to 360°. At the same time, the load impedance value yielding the maximum efficiency can be computed from (2) [9].

In this research, the harvester circuit is expected to be placed on the human body. However, because of regulation issues related to human subject research, a bottle of water was adopted as the substitute material for the human forearm for the preliminary measurements. In reality, the human body has different electrical properties compared to the water. Therefore, in order to imitate the human body effects more accurately, a phantom should be used in future research efforts. However, as a first-order approximation and as a proof-of-concept of the wearable near-field RF energy harvesting, and without loss of generality, a spindle-shape 20-cm-tall water bottle, which has the smallest diameter of 17.5 cm at the middle and the largest diameter of 23 cm at the top and bottom, was used. In order to mimic the two-way talk radio, a stubby UHF antenna, RAN4033 from Motorola, which has similar physical dimension to the one on the two-way talk radio, was placed at the bottom of the water bottle and was used for the S-parameter measurements. The E-field receiver was wrapped around the bottle at a distance of 7 cm from the bottom of the bottle in a configuration equivalent to the handheld two-way radio and the "7 cm" position of the harvester in Fig. 7(a). Similarly, the H-field receiver was placed at 2 cm away from the bottom of the water bottle which is equivalent to the "2 cm" position in Fig. 7. The measured S-parameters for the transmitting monopole and for the E- and H-field receivers are plotted in Fig. 10 for this specific configuration. Using this data in (1) and (2), the maximum potential power transfer efficiency was determined to be 2.57% and 7.55% for the E-field and the H-field receivers, respectively. For the E-field harvester circuit, the maximum possible transferred power from the 2.2 W transmitter, 56.2 mW, and the load impedance at the maximum power transfer condition, $202 - j90$, were determined from (1) and (2), respectively. From the same equations, the H-field harvester maximum possible transferred power of, 166.0 mW, and the load impedance at the maximum power transfer condition, $10.7 - j4.6$, were computed. In order to maximize the output voltage with the minimum possible circuit size, a single-stage Dickson voltage doubler with one Schottky diode chip, Avago HSMS282C, was used as the rectifier. Also in order to keep the size of harvester small, an L-shaped LC network was adopted as the matching circuit. The circuit was initially designed with the Advanced Design System (ADS), and the matching circuit was fine-tuned during measurements. The configuration of the E and H-field rectifier prototypes is shown in Fig. 11(a) and (b), respectively.

IV. Measurement Results

A. RF-DC Conversion Efficiency Measurements

The output voltage measurements were initially conducted with an RDU2020 handheld radio by arranging the harvester and the radio on the side of the water bottle in a configuration similar to the one on the human arm holding the radio as shown in Figs. 12(a) and 13(a). The output voltage was measured by changing the load resistance of the circuit in the range

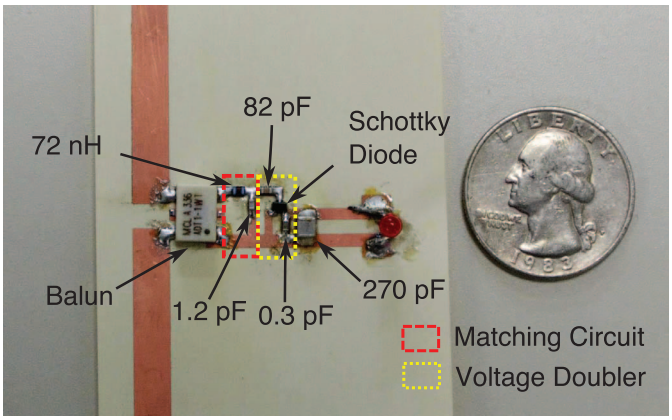

(a)

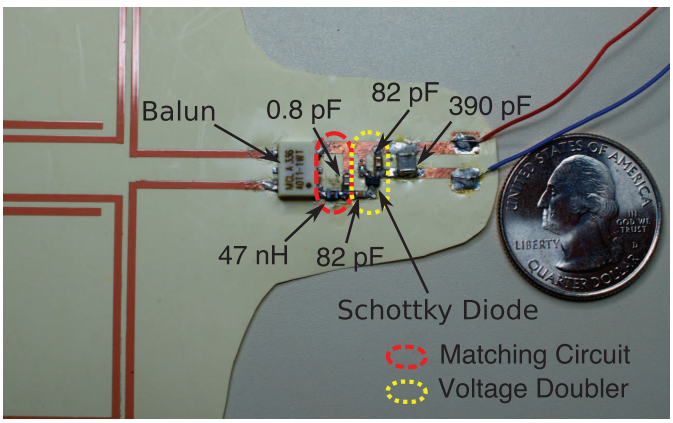

(b)

Fig. 11. RF-dc conversion circuit topology for the wearable (a) E-filed energy harvester. (b) H-filed energy harvester.

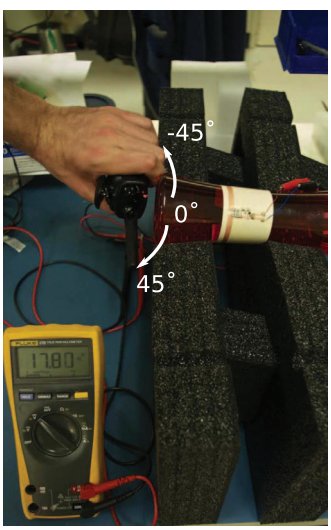

(a)

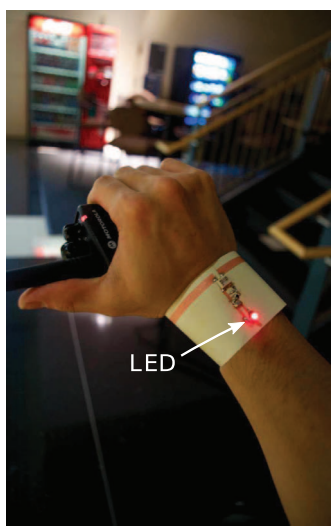

(b)

Fig. 12. (a) Open voltage measurement of E-field harvester with an on-bottle setup. (b) Operation verification of the E-field harvester on the wrist.

of 100 to 6800 Ω, which fully covers the optimal load resistance value range of 1800 to 3000 Ω from ADS simulation. The input power is assumed to be 56.2 mW (17.5 dBm) for the E-field harvester, and 166.0 mW (22.2 dBm) for the H-field

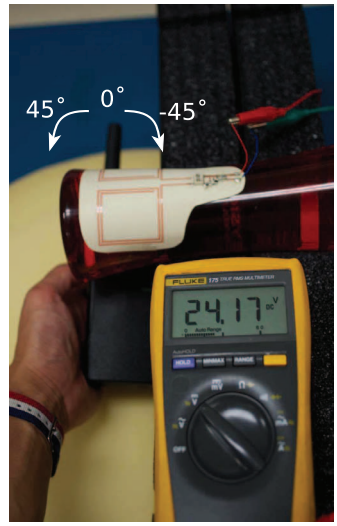

(a)

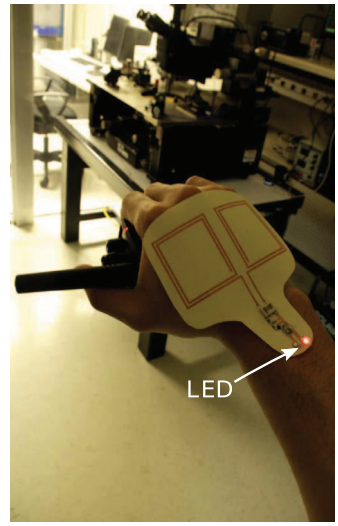

(b)

Fig. 13. (a) Open voltage measurement of H-field harvester with an on-bottle setup. (b) Operation verification of the H-field harvester on the hand.

harvester from the input power estimation based on the S-parameter measurements. The estimated RF-dc conversion efficiency from both the simulations and the measurements for E- and H-field harvesters as a function of the load resistance are depicted in Figs. 14 and 15, respectively. During the simulation, the matching circuit and the load resistance are optimized to achieve the highest dc output power for the estimated RF input power using ideal circuit components. The RDU two-way talk radios can potentially switch the transmitting power to 1 and 4 W. Therefore, the RF-dc conversion efficiencies when the input power is halved and doubled without changing the matching circuit design are also depicted in Figs. 14 and 15. According to the simulation results, the maximum RF-dc conversion at every input power level observation is almost the same for both E- and H-field harvesters, and the optimal load resistance value shifts slightly lower as the input power increases. These are because the input power is pretty high and the junction capacitance of the diodes, which is input power dependent at low input power levels, is negligibly small, and only the real part of the diode impedance changes as the input power levels are varied. The sharp decrease in the RF-dc conversion efficiency for high load resistance values at high input power levels happens because the output voltage becomes larger than the breakdown voltage of the diode, resulting in limiting effects. As a result of the measurements, the estimated maximum RF-dc conversion efficiency of 76.3% was achieved for the 1772 Ω load resistance for E-field harvester and 88.5% was achieved for the 2996 Ω load resistance for H-field harvester based on the measurements. The reason why the simulation and measurement results for the E- and H-field harvester show minor disagreements in terms of the optimal load resistance is assumed to be the fact that the estimated input power from the S-parameters measurement is lower than the actual input power, practically causing some amount of mismatch between the receiver and the RF-dc conversion circuit. Also, the difference between the ideal and the actual lumped components could be the cause of the higher loss in the measurement. As depicted in Figs. 12(b) and 13(b), an operation test using a LED was conducted by replacing the load

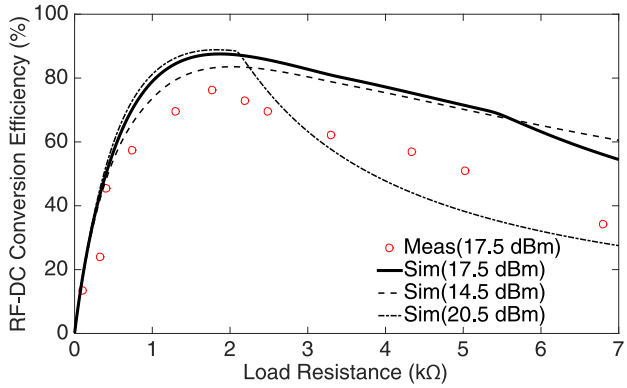

Fig. 14. Simulated and estimated RF-dc conversion efficiency values from S-parameters measurements and the measured output dc power from E-field harvester prototype with respect to load resistance.

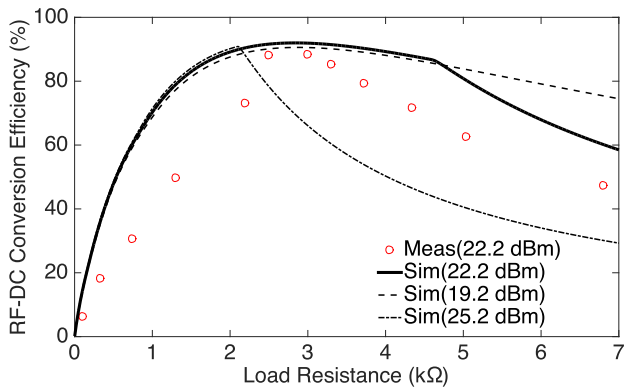

Fig. 15. Simulated and estimated RF-dc conversion efficiency values from S-parameters measurements and the measured output dc power from H-field harvester prototype with respect to load resistance.

resistance with a LED while mounting the prototype of E-field harvester on the wrist, and sticking the H-field harvester prototype on the back of the hand. As a result, the LED was successfully turned on utilizing only the harvested energy from the handheld radio under the typical radio operation conditions for both scenarios [9], [10].

B. Comparison of Inkjet Printing Masking and Inkjet Printed Conductive Traces

Based on the assumption that the traces for the RF-dc conversion circuit are electrically small compared to the wavelength at 464 MHz and that the difference in substrate materials do not significantly affect the operation of the circuit, the same circuit design of the inkjet-printed masking prototype was adopted for the conductive inkjet-printed H-field harvester circuit. In order to avoid having the problem of cracking in the printed conductive traces, the conductive epoxy paste used for the electrical connection of lumped components was laminated with a thin epoxy glue layer as depicted in Fig. 16. In order to determine the effect of epoxy lamination on the performance of the harvester circuit, the output dc power from the H-field harvester before and after the lamination were measured on a flat sponge, whose thickness is 35 mm by arranging the hand-held radio on the back side of the sponge. The results are depicted in Fig. 17, verifying that there is no significant difference in performance

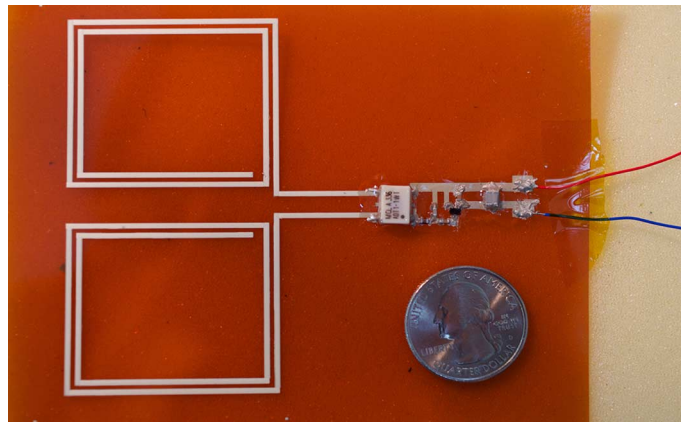

Fig. 16. H-field harvester prototype using inkjet-printed conductive traces after lamination with an epoxy glue.

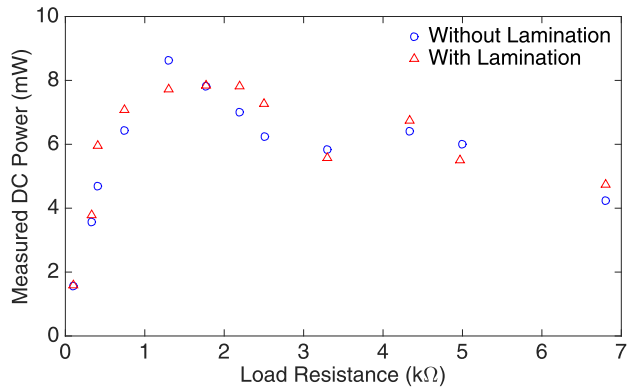

Fig. 17. Output dc power of the conductive inkjet-printed H-field harvester prototype with and without lamination under flat conditions.

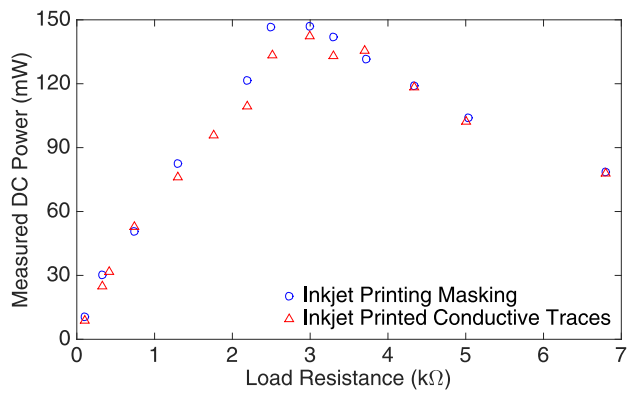

Fig. 18. Output dc power from the prototypes of H-field harvester using inkjet printing masking and inkjet-printed conductive traces under "on bottle" bent/flex conditions.

due to the lamination. As a final test, the output power from the conductive inkjet-printed H-field harvester was measured on the water bottle to compare the performance of harvesting with the inkjet printing masking H-field harvester under bent/flex conditions. The output dc power with respect to the load resistance for both inkjet printing masking and inkjet-printed conductive traces are shown in Fig. 18, showing a very good agreement, while the open output voltage of the conductive inkjet-printed H-field harvester is shown in Fig. 19.

Fig. 19. Open voltage measurement of the conductive inkjet-printed H-field harvester with an on-bottle setup.

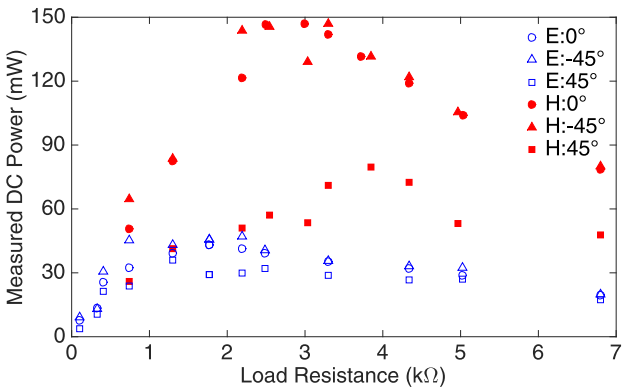

Fig. 20. Output dc power from E-field and H-field harvester prototypes using LCP substrate on bottle at different misalignment angles.

C. Effect of Misalignment on Harvesting Performance

Potential misalignment between the hand-held radio and harvester would possibly degrade the performance of harvesters. It is known that the range of motion of a wrist is about 40° for both flexion and extension, and 40° of combined radial-ulnar deviation [23]. In order to investigate the effect of misalignment for wearable harvesters, output dc power measurements under the condition of $\pm 45°$ aligned positions are conducted. The direction of the misaligning rotation for the E- and the H-field harvester are depicted in Figs. 12(a) and 13(a), respectively. The output dc power with respect to the load resistance at each angle is plotted in Fig. 20. Assuming that the maximum degradation in input power occurs at the highest misalignment angle, the E-field harvester features a maximum of 49.2% output dc power variation compared to the 0° condition. Similarly, the maximum output dc power variation for H-field harvester associated with misalignment is 63.5%. The reason why the dc power of the H-field at $-45°$ is much larger than at 45° can be attributed to the fact that the distance between the antenna and the receiver in the harvester is longer in the case of 45° than in the case of $-45°$ because of the extra transmission line length between the rectangular traces and the balun even if it looks like a symmetric shape. From these results, it can be concluded that alignment is critical to achieve a high RF-dc conversion efficiency with wearable harvester circuit. During the actual on-body operation, it can be assumed that the relative geometrical orientations among the transmitter, the harvester and the hand can significantly change the coupling and the matching conditions a lot. In order to overcome this issue, a receiver with misalignment-correction capabilities has to be used. Also, the design of a matching circuit for wide operation power range, for example a real-time active matching circuit, can be introduced to compensate the effect of the misalignment [24].

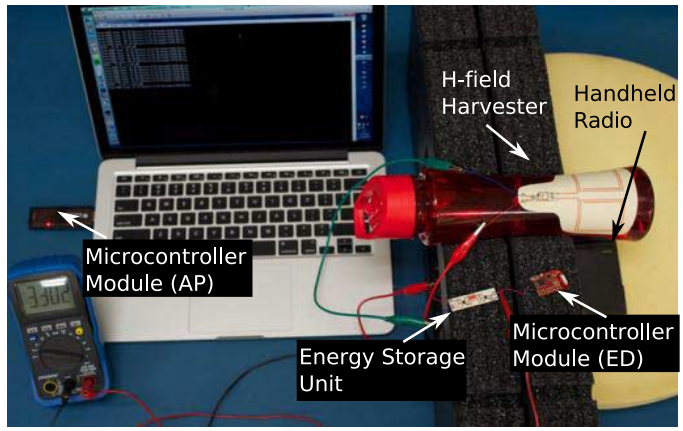

Fig. 21. Setup for the operation test of H-field harvester using a microcontroller module.

D. Operation Test Using Microcontroller Module

One of the fundamental motivations of this research is to overcome the problem of the "cold start" of ICs by introducing a wearable flexible near-field energy harvesting circuit. In order to test the applicability of the proposed harvester to wireless autonomous sensing devices, an operation test using microcontroller modules was conducted. The setup for the operation verification is depicted in Fig. 21. The harvested energy was stored in the energy storage unit, which was composed of a 1000 μF Tantulum capacitor and voltage regulators to protect the capacitor and the microcontroller module. The MSP430 base microcontroller unit, eZ430-RF2500 provided by Texas Instruments, was used as the Access Point (AP) and the End Device (ED). The module has the functionality of wireless communication at 2.45 GHz, while functioning as a thermometer utilizing an analog-to-digital converter (ADC). The operation and the duty cycle of the ED, which was powered by an H-field harvester, were optimized to realize a low power consumption. The current flow to the ED when the module was powered by a 3.3 V voltage source was measured by using a digital oscilloscope, Tektronix DPO7354, as is plotted in Fig. 22, which clearly shows an initial operation state and a normal operation state. During the initial operation, the ED is sequentially performing the following four tasks; initializes the microcontroller, establishes communication between the ED and the AP, acquires the temperature data using ADC and sends the data back to the AP by transmitting RF signals. Similarly, the ED acquires the temperature data and sends the data to the AP during the normal operation. In order to start up the operation, it requires about 986 μJ of energy at the supply voltage of 3.3 V. At the normal operation, the module requires about 193 μJ of energy for every measurement. These values are computed by integrating the instant power consumption during the initial and the normal operation states obtained from the previous oscilloscope measurement data. Also,

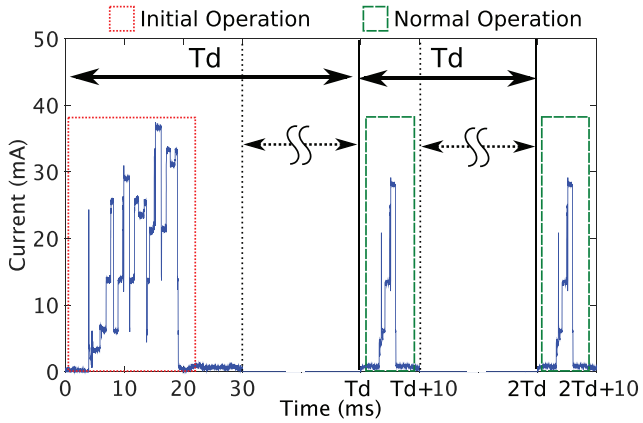

Fig. 22. Measured microcontroller module (ED) current flow in the initial operation state and in the normal operation state.

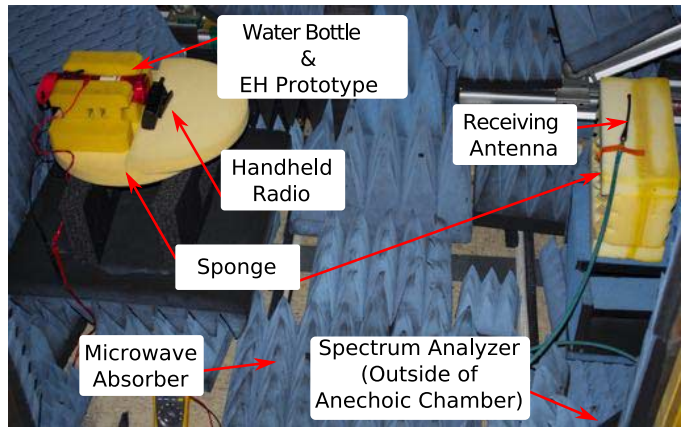

Fig. 23. Received power measurement in an anechoic chamber.

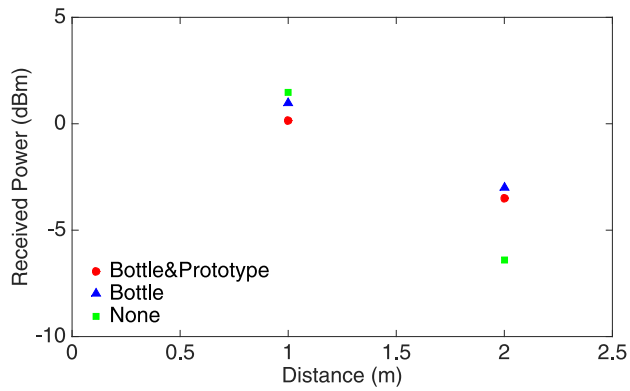

Fig. 24. Effect of harvester prototype on received communication power.

the initial operation requires the maximum instantaneous power of 123.75 mW, which is about 1.32 times larger than in the normal operation. Without loss of generality, we assume that the temperature acquisition and data transmission are conducted at an arbitrary interval, which is represented as Td in the Fig. 22. For the operation verification test, the duty cycle was chosen as 5 s for practical proof-of-concept purposes. After each measurement, the ED stays in low power consumption mode until the next measurement, and consumes about 4.3 μW of power according to the application note [25]. As a result of the verification test, the ED turns on within 1 s from the "cold start" and starts sending the data once the two-way talk radio was turned on. After 1 s of charging, the ED can repeat the normal operation for three to five times at the duty-cycle of 5 s. The number of operations was confirmed by counting the number of the communication logs shown on the computer. It can be assumed that the variation in the number of operations was caused by the variance in the stored energy in the capacitor after the charging because the dc power from the harvester varies depending on the load resistance and the misalignment. Also, the required energy for the ED to establish the communication with the AP changes depending on how fast they establish the communication link. The number of "autonomous" operations could not exceed 5 times even if the charging time was increased, which is implying that the capacitor in the energy storage unit had been already saturated after 1 s of charging. Therefore, it is assumed that it would be possible to extend the operation time by introducing a high-capacity energy storage device, such as a lithium ion battery.

E. Effect of Harvester on the Two-Way Radio Communication Quality

Since the energy harvester circuit is utilizing energy which is originally expected to be used for communication signals, it could possibly degrade the quality of communication. In order to specify the effects of the energy harvesting circuit on the handheld radio communication performance, the received power, which represents the quality of communication, was measured in the anechoic chamber for the following three different conditions at 1 and 2 m separation distances between the transmitter and the receiving antenna: i) the harvester prototype on the water bottle is placed in the proximity of the radio as is Fig. 12; ii) only the water bottle is placed near the radio; and iii) both the water bottle and the harvester prototype are removed from the vicinity of the radio. The measurement setup is shown in Fig. 23 [9] involving one prototype of the E-field harvester. For the measurement, one prototype of the E-field harvester was used. The receiving antenna was a monopole antenna, ANT-433-CW-QW from Linx Technologies Inc,. The measurement results are depicted in Fig. 24, verifying that the difference in the received power between the case (i) and the case (ii) at two different separation distances in the far field were quite small, meaning that the effects of adding a wearable harvester to a hand holding a radio are almost negligible. On the other hand, the difference between case (ii) and (iii) is quite significant, which implies that the effect of harvesting is small compared to the effect of existence of water bottle, which is probably causing fading. Therefore, it can be concluded that the degradation of the communication performances of the two-way talk radio by the presence of the energy harvesting circuit is much smaller compared to the human body effect.

V. Conclusions

In this paper, the design and additive manufacturing fabrication process of flexible near-field ambient energy harvesting circuits for wearable sensor device applications is discussed. Numerous proof-of-concept circuit prototypes were fabricated through the combination of conductive traces realized with

inkjet printing masking and conductive inkjet printing technologies with lumped circuit components. The input power for the RF-dc conversion circuit was analytically estimated from the measured S-parameters, and the maximum output power levels of 146.9 mW and 43.2 mW were achieved with H-field and E-field harvesters, respectively. Numerous operation tests of E- and H-field energy harvesters were conducted by utilizing a LED and a microcontroller communication module under on-body and on-bottle bent/flex conditions, and verified the successful powering of both modules utilizing only the energy from the two-way talk radio. These very promising preliminary results suggest the wide potential applicability of the proposed inkjet-printed flexible energy harvesters to a variety of wearable biomonitoring, WBAN and Internet of Things applications.

REFERENCES

[1] M. Pinuela, P. D. Mitcheson, and S. Lucyszyn, "Ambient RF energy harvesting in urban and semi-urban environments," *IEEE Trans. Microw. Theory Tech.*, vol. 61, no. 7, pp. 2715–2726, Jul. 2013.

[2] R. J. Vyas, B. B. Cook, Y. Kawahara, and M. M. Tentzeris, "E-WEHP: A batteryless embedded sensor-platform wirelessly powered from ambient digital-TV signals," *IEEE Trans. Microw. Theory Tech.*, vol. 61, no. 6, pp. 2491–2505, Jun. 2013.

[3] J. A. Paradiso and T. Starner, "Energy scavenging for mobile and wireless electronics," *IEEE Pervasive Comput.*, vol. 4, no. 1, pp. 18–27, Jan. 2005.

[4] X. Wang and A. Mortazawi, "Medium wave energy scavenging for wireless structural health monitoring sensors," *IEEE Trans. Microw. Theory Tech.*, vol. 62, no. 4, pp. 1067–1073, Apr. 2014.

[5] S. Kim, R. Vyas, J. Bito, K. Niotaki, A. Collado, A. Georgiadis, and M. Tentzeris, "Ambient RF energy-harvesting technologies for self-sustainable standalone wireless sensor platforms," *Proc. IEEE*, vol. 102, no. 11, pp. 1649–1666, Nov. 2014.

[6] A. Kurs, A. Karalis, R. Moffatt, J. D. Joannopoulos, P. Fisher, and M. Soljačić, "Wireless power transfer via strongly coupled magnetic resonances," *Science*, vol. 317, no. 5834, pp. 83–86, Jul. 2007.

[7] R. Want, "An introduction to RFID technology," *IEEE Pervasive Comput.*, vol. 5, no. 1, pp. 25–33, Jan. 2006.

[8] P. V. Nikitin, K. V. S. Rao, and S. Lazar, "An overview of near field UHF RFID," in *Proc. 2007 IEEE Int. Conf. on RFID*, Grapevine, TX, USA, Mar. 2007, pp. 167–174.

[9] J. Bito, J. G. Hester, and M. M. Tentzeris, "Ambient energy harvesting from a two-way talk radio for flexible wearable devices utilizing inkjet printing masking," in *2015 IEEE MTT-S Int. Microwave Symp. Dig.*, Phoenix, AZ, USA, May 2015, pp. 1–4.

[10] J. Bito and M. Tentzeris, "A novel flexible wearable magnetic energy harvester utilizing inkjet masking techniques," in *Proc. 2015 IEEE Antennas and Propagation Soc. Int. Symp.*, Vancouver, BC, Canada, Jul. 2015.

[11] L. Yang, A. Rida, R. Vyas, and M. M. Tentzeris, "RFID tag and RF structures on a paper substrate using inkjet-printing technology," *IEEE Trans. Microw. Theory Tech.*, vol. 55, no. 12, pp. 2894–2901, Dec. 2007.

[12] B. S. Cook, J. R. Cooper, and M. M. Tentzeris, "Multi-layer RF capacitors on flexible substrates utilizing inkjet printed dielectric polymers," *IEEE Microw. Wireless Compon. Lett.*, vol. 23, no. 7, pp. 353–355, Jul. 2013.

[13] B. S. Cook, C. Mariotti, J. R. Cooper, D. Revier, B. K. Tehrani, L. A. L. Roselli, and M. M. Tentzeris, "Inkjet-printed, vertically-integrated, high-performance inductors and transformers on flexible LCP substrate," in *2014 IEEE MTT-S Int. Microwave Symp. Dig.*, Tampa, FL, USA, Jun. 2014, pp. 1–4.

[14] J. G. Hester, Y. Fang, and M. M. Tentzeris, "Inkjet-printed, flexible, high performance, carbon nanomaterial based sensors for ammonia and DMMP gas detection," in *Proc. 45th Eur. Microwave Conf.*, Paris, France, Sep. 2015.

[15] A. C. Arias, J. D. MacKenzie, I. McCulloch, J. Rivnay, and A. Salleo, "Materials and applications for large area electronics: Solution-based approaches," *Chem. Rev.*, vol. 110, no. 1, pp. 3–24, Jan. 2010.

[16] J. G. Hester, S. Kim, J. Bito, T. Le, J. Kimionis, D. Revier, C. Saintsing, S. Wenjing, B. Tehrani, A. Traille, B. S. Cook, and M. M. Tentzeris, "Additively manufactured nanotechnology and origami-enabled flexible microwave electronics," *Proc. IEEE*, vol. 103, no. 4, pp. 583–606, Apr. 2015.

[17] Y. Kawahara, S. Hodges, B. S. Cook, C. Zhang, and G. D. Abowd, "Instant inkjet circuits: Lab-based inkjet printing to support rapid prototyping of UbiComp devices," in *Proc. 2013 ACM Int. Joint Conf. on Pervasive and Ubiquitous Computing (UbiComp '13)*, New York, NY, USA, Sep. 2013, pp. 363–372.

[18] B. K. Tehrani, J. Bito, B. S. Cook, and M. M. Tentzeris, "Fully inkjet-printed multilayer microstrip and T-resonator structures for the RF characterization of printable materials and interconnects," in *2014 IEEE MTT-S Int. Microwave Symp. Dig.*, Tampa, FL, USA, Jun. 2014, pp. 1–4.

[19] J. Bito, B. Tehrani, B. Cook, and M. Tentzeris, "Fully inkjet-printed multilayer microstrip patch antenna for Ku-band applications," in *Proc. 2014 IEEE Antennas and Propagation Soc. Int. Symp.*, Memphis, TN, USA, Jul. 2014, pp. 854–855.

[20] S. Kim, J. Bito, J. Soyeon, A. Georgiadis, and M. M. Tentzeris, "A flexible hybrid printed RF energy harvester utilizing catalyst-based copper printing technologies for far-field RF energy harvesting applications," in *2015 IEEE MTT-S Int. Microwave Symp. Dig.*, Phoenix, AZ, USA, May 2015, pp. 1–4.

[21] Technical Data Sheet Nanosilver Conductive Ink EMD5730 SunChemical, 2013.

[22] B. Cook and A. Shamim, "Inkjet printing of novel wideband and high gain antennas on low-cost paper substrate," *IEEE Trans. Antennas Propag.*, vol. 60, no. 9, pp. 4148–4156, Sep. 2012.

[23] J. Ryu, W. P. Cooney, III, L. J. Askew, K. N. An, and E. Y. S. Chao, "Functional ranges of motion of the wrist joint," *J. Hand Surgery*, vol. 16, no. 3, pp. 409–419, May 1991.

[24] J. Bito, J. Soyeon, and M. M. Tentzeris, "A real-time electrically controlled active matching circuit utilizing genetic algorithms for biomedical WPT applications," in *Proc. 2015 IEEE Wireless Power Transfer Conf.*, Boulder, CO, USA, May 2015, pp. 1–4.

[25] M. Morales and Z. Shivers, *Appl. Note SLAA378D Wireless Sensor Monitor Using the eZ430-RF2500*. Dallas, TX, USA: Texas Instruments, 2011.

Jo Bito (S'13) received the B.S. degree in electrical and electronic engineering from Okayama University, Okayama, Japan in 2013. From 2010 to 2011 he was with the International Programs in Engineering (IPENG), and studied at University of Illinois Urbana-Champaign, Champaign, IL, USA. He is currently pursuing the Ph.D. degree in electrical and computer engineering at the Georgia Institute of Technology, Atlanta, GA, USA.

He is now a Research Assistant in the ATHENA research group. His research interests include the application of inkjet printing technology for flexible and wearable electronics, RF energy harvesting, and wireless power transfer systems. He is a recipient of the Japan Student Services Organization (JASSO) long-term scholarship from 2013.

Jimmy G. Hester (S'14) spent two intense preparation years studying fundamental chemistry, math, and physics after which he was admitted in INP Toulouse, ENSEEIHT where he received the graduate degree and M.S degree in electrical and signal processing engineering, majoring in radio frequency electronics, in 2012 and 2014, respectively. He received the M.S. degree in electrical and computer engineering from the Georgia Institute of Technology, Atlanta, GA, USA, in 201, where he is now working, as a Research Assistant in the ATHENA group, toward the Ph.D. degree in electrical and computer engineering.

His research interests lie at the interface between radio frequency (RF) engineering and material science, in the form of flexible electronics technologies and nanotechnologies. Recently, he has been working toward the use of carbon nanomaterials applied to inkjet-printed RF sensing components for flexible low cost ubiquitous gas sensing applications. His work covers the entire development process, from the development of inkjet inks, improvement of fabrication methods, sensor component design, high-frequency characterization, and environmental testing to the design, simulation, and fabrication of the RF system embedding the sensor.

Manos M. Tentzeris (S'89–M'92–SM'03–F'10) received the Diploma Degree in electrical and computer engineering from the National Technical University of Athens ("Magna Cum Laude"), Athens, Greece and the M.S. and Ph.D. degrees in electrical engineering and computer science from the University of Michigan, Ann Arbor, MI, USA.

He is currently a Professor with School of Electrical and Computer Engineering, Georgia Institute of Technology (Georgia Tech), Atlanta, GA, USA. He has published more than 550 papers in refereed journals and conference proceedings, five books ,and 23 book chapters. He has helped develop academic programs in highly integrated/multilayer packaging for radio frequency (RF) and wireless applications using ceramic and organic flexible materials, paper-based RFIDs and sensors, biosensors, wearable electronics, 3-D/4-D/inkjet-printed electronics, "green" electronics, energy-harvesting and wireless power transfer systems, NFC systems, nanotechnology applications in RF, origami-folded electromagnetics, microwave MEMs, SOP-integrated (UWB, multiband, mmW, conformal) antennas and heads the ATHENA research group (20 researchers). He has served as the Head of the GT-ECE Electromagnetics Technical Interest Group, as the Georgia Electronic Design Center Associate Director for RFID/Sensors research from 2006–2010 and as the Georgia Tech NSF-Packaging Research Center Associate Director for RF Research and the RF Alliance Leader from 2003–2006. He was a Visiting Professor with the Technical University of Munich, Germany for the summer of 2002, a Visiting Professor with GTRI-Ireland in Athlone, Ireland for the summer of 2009, and a Visiting Professor with LAAS-CNRS in Toulouse, France for the summer of 2010. He has given more than 100 invited talks to various universities and companies all over the world.

Dr. Tentzeris was the recipient/co-recipient of the 2015 IET Microwaves, Antennas and Propagation Premium Award, the 2014 Georgia Tech ECE Distinguished Faculty Achievement Award, the 2014 IEEE RFID-TA Best Student Paper Award, the 2013 IET Microwaves, Antennas and Propagation Premium Award, the 2012 FiDiPro Award in Finland, the iCMG Architecture Award of Excellence, the 2010 IEEE Antennas and Propagation Society Piergiorgio L. E. Uslenghi Letters Prize Paper Award, the 2011 International Workshop on Structural Health Monitoring Best Student Paper Award, the 2010 Georgia Tech Senior Faculty Outstanding Undergraduate Research Mentor Award, the 2009 IEEE Transactions on Components and Packaging Technologies Best Paper Award, the 2009 E.T.S.Walton Award from the Irish Science Foundation, the 2007 IEEE APS Symposium Best Student Paper Award, the 2007 IEEE IMS Third Best Student Paper Award, the 2007 ISAP 2007 Poster Presentation Award, the 2006 IEEE MTT Outstanding Young Engineer Award, the 2006 Asian-Pacific Microwave Conference Award, the 2004 IEEE Transactions on Advanced Packaging Commendable Paper Award, the 2003 NASA Godfrey "Art" Anzic Collaborative Distinguished Publication Award, the 2003 IBC International Educator of the Year Award, the 2003 IEEE CPMT Outstanding Young Engineer Award, the 2002 International Conference on Microwave and Millimeter-Wave Technology Best Paper Award (Beijing, CHINA), the 2002 Georgia Tech-ECE Outstanding Junior Faculty Award, the 2001 ACES Conference Best Paper Award and the 2000 NSF CAREER Award and the 1997 Best Paper Award of the International Hybrid Microelectronics and Packaging Society. He was the TPC Chair for IEEE IMS 2008 Symposium and the Chairof the 2005 IEEE CEM-TD Workshop and he is the Vice-Chair of the RF Technical Committee (TC16) of the IEEE CPMT Society.He is the founder and chair of the RFID Technical Committee (TC24) of the IEEE MTT Society and the Secretary/Treasurer of the IEEE C-RFID. He is an Associate Editor of IEEE TRANSACTIONS ON MICROWAVE THEORY AND TECHNIQUES, IEEE TRANSACTIONS ON ADVANCED PACKAGING, and the *International Journal on Antennas and Propagation*. He is a member of URSI-Commission D, a member of MTT-15 committee, an Associate Member of the European Microwave Association, a Fellow of the Electromagnetic Academy, and a member of the Technical Chamber of Greece. He served as one of the IEEE Microwave Theory and Techniques Society Distinguished Microwave Lecturers from 2010–2012, and he is currently serving as the IEEE C-RFID Distinguished Lecturer.